CHEMISTRY OF MATERIALS

Article

pubs.acs.org/cm

Silver Nanorice Structures: Oriented Attachment-Dominated Growth, High Environmental Sensitivity, and Real-Space Visualization of Multipolar Resonances

Hongyan Liang,[†] Haiguang Zhao,[†] David Rossouw,[⊥] Wenzhong Wang,[‡] Hongxing Xu,*[,§,▽] Gianluigi A. Botton,[⊥] and Dongling Ma*[,†]

[†]INRS—Énergie, Matériaux et Télécommunications, Université du Québec, 1650 Boulevard Lionel-Boulet, Varennes (QC), J3X 1S2, Canada

[⊥]Department of Materials Science and Engineering, McMaster University, 1280 Main Street W. Hamilton ON, L8S 4L7, Canada

[‡]School of Science, Minzu University of China, Beijing 100081, People's Republic of China

[§]Institute of Physics, Chinese Academy of Sciences, Beijing 100190, People's Republic of China

[▽]Division of Solid State Physics, Lund University, Lund, 22100, Sweden

Supporting Information

ABSTRACT: We have synthesized and investigated the anisotropic growth of interesting silver nanorice. Its growth is kinetically controlled at 100 °C, and both oriented attachment and Ostwald ripening are involved, with the former growth mode dominating the anisotropic growth of the nanorice along the ⟨111⟩ direction. This one-directional growth is initiated by an indispensable seed-selection process, in which oxygen plays a critical role in oxidatively etching twinned silver crystals. The inhibition of this process by removing oxygen essentially blocks the nanorice growth. Although increasing reaction temperature to 120 °C accelerates the one-dimensional growth along the ⟨111⟩ direction, further temperature increase to 160 °C makes the oriented attachment dominated one-directional growth disappear; instead, the diffusion-controlled two-dimensional growth leads to the emergence of highly faceted truncated triangular and hexagonal plates mainly bound by low energy faces of {111}. Interestingly, we also found that the longitudinal surface plasmon resonance of the nanorice structures is highly sensitive to the refractive index of surrounding dielectric media, which predicts their promising applications as chemical or biological sensors. Moreover, the multipolar plasmonic resonances in these individual nanorice structures are visualized in real space, using high-resolution electron energy-loss spectroscopy.

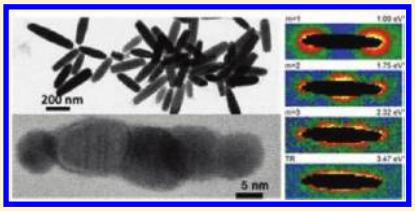

KEYWORDS: *silver nanorice, growth mechanism, oriented attachment, surface plasmon resonance, multipolar plasmonic resonance, electron energy-loss spectroscopy*

INTRODUCTION

Metal nanostructures have attracted much attention and have been extensively studied for many decades, because of their broad applications in catalysis, biological labeling, transistors, optoelectronics, and surface-enhanced spectroscopy.[1−4] Silver nanocrystals have attracted significant attention, because of the possibility of systematically controlling their size and shape in synthesis and thereby their localized surface plasmon resonance (SPR), as well as a series of important applications in various areas, such as surface-enhanced Raman spectroscopy and refractive index sensitivity analysis.[5−7] The solution-phase reliable synthesis of silver nanocrystals with well-controlled shape and size in high yield is important in creating novel platforms for the investigation of morphology-dependent optical properties. It has been shown that silver nanocrystals with various shapes, such as nanodisks,[8] nanowires,[9] nanobars,[10] nanoplates,[11] nanorice structures,[12] nanospheres,[13] and nanoparticles (NPs)[14] can be synthesized in relatively high yield.

Recently, Xia's group and other researchers have demonstrated the large-scale synthesis of silver nanostructures with controllable sizes and shapes via a polyol method, where the liquid polyol acts not only as a solvent for the precursors, but also as a mild reducing reagent.[10,12−17] It was found that the morphologies of both nuclei and products were highly affected by trace amounts of additives (such as NaCl and NaBr), because of their etching capability.[10,16] On the basis of this finding, many anisotropic silver nanostructures, such as nanowires,[9] nanobars,[10] and nanocubes[17] have been successfully synthesized in ethylene glycol (EG) solution. Recently, we have reported the preparation of silver nanorice structures with uniform shape using polyethylene glycol 600 (PEG 600) instead of EG.[12] To the best of our knowledge, the nanorice with stacking faults of the face-centered cubic (FCC) phase coexisting with the hexagonal close-packed (HCP) phase at the

Received: March 2, 2012
Revised: May 10, 2012
Published: May 29, 2012

   dx.doi.org/10.1021/cm3006875 | *Chem. Mater.* 2012, 24, 2339−2346

tip was found for the first time in silver nanocrystals. More importantly, high-order SPR modes in individual silver nanorice structures were revealed by means of dark-field scattering spectroscopy.[18] However, the growth mechanism of these silver nanorice structures has not been investigated and the understanding on key shape-determining parameters remains very limited. Thus, the ability to understand these aspects can potentially lead to better control over the reproducibility, shape uniformity, and yield on the shape-directed synthesis of the nanorice structures. In addition, the optical properties of these novel nanorice structures require further investigation before they can be explored for practical applications. Moreover, it is desirable yet challenging to image the plasmonic resonance in the spatial domain in order to provide insight into the light/matter interactions at the nanometer scale and understand if these nanostructures behave qualitatively different from more-simple nanostructures. Given these gaps in information and understanding, in this paper, we therefore investigate the growth process of the silver nanorice structures, study how atmosphere and temperature affect the formation of the staggered silver nanorice structures, and, based on these results, further elucidate their growth mechanism. We also examine the sensitivity of the localized plasmon resonance to the variation of the refractive index of surrounding media. Furthermore, from real-space mapping of the multipolar plasmonic resonances in individual nanorice structures using electron energy-loss spectroscopy (EELS) imaging, we compare their optical response to observations in simple silver cylinders.

EXPERIMENTAL SECTION

Materials. $AgNO_3$ (99.8%) and poly(vinyl pyrrolidone) (PVP) with an average molecular weight of 40 000 (PVP K30) were achieved from Sigma–Aldrich, Inc. PEG 600 was purchased from Xilong Chemical Industry Incorporated Co., Ltd. All chemicals were used as-received. Deionized water with a resistance of 18 MΩ cm was used in all cases.

Synthesis of Silver Nanocystals. The stock solution was first prepared by dissolving PVP (1.11 g) in 100 mL of PEG under stirring, followed by the addition of 1 mL of 2 M $AgNO_3$ aqueous solution. The solution was allowed to incubate at room temperature for at least one month. The silver nanocrystals then were synthesized according to our previously reported procedures.[12] In a typical synthesis, 15 mL of stock solution in a 100-mL flask was heated to 70 °C and kept at that temperature in an oil bath for ∼2 h (stage I). When the yellow color disappeared, the nearly colorless solution was further heated at certain temperatures for growth (stage II), which went through a series of color changes. No intentional control over the atmosphere was exerted in these operations. At various time intervals, aliquots of the reaction mixture were taken from the reaction solution by a glass pipet and quenched by cold water to room temperature for immediate absorption measurements or for other characterizations after product purification. To minimize the temperature perturbation during sampling, the glass pipet was preheated for 20 s by suspending it above the reaction solution before it was immersed into the reaction solution.

In order to examine the effect of oxygen on the synthesis of the silver nanocrystals, the reaction was also performed under the protection of N_2 for comparison. Two different conditions were applied. In one scenario, 15 mL of the stock solution was first bubbled with N_2 under vigorous stirring for 30 min and then vacuumed for 20 min. After that, the synthesis followed the above-described procedures (stages I and II) with the only exception being under N_2. In the other scenario, the N_2 protection was only applied to stage II.

The product was purified by centrifugation at 11 000 rpm for 20 min after adding certain amounts of acetone. The precipitates were then dispersed in deionized water or ethanol and repeatedly centrifuged for several more times to remove excess PEG 600 and PVP. Finally, the sample was dispersed in ethanol for further characterization.

Preparation of a Monolayer of Silver Nanorice Structures on a Modified Glass Substrate. A silver nanorice structure monolayer was deposited on a (3-aminopropyl) trimethoxysilane-coated glass substrate by exposing it to the diluted nanorice alcohol solution for 2 h. The substrate then was rinsed with alcohol and dried by N_2.

Characterization. Extinction spectra of the samples were acquired with a Cary 5000 ultraviolet–visible–near-infrared (UV-Vis-NIR) spectrophotometer (Varian) at a scan speed of 600 nm/min. The SPR sensitivity of the nanorice structures was studied by immersing the monolayer of isolated nanorice structures immobilized on a glass slide into solvents with different refractive indices and monitoring the variation of their UV-Vis-NIR spectra. Scanning electron microscopy (SEM) images of silver nanocrystals were obtained using a HITACHI Model S-4800 SEM system. Low- and high-resolution transmission electron microscopy (TEM) images were taken using a JEOL Model 2100F microscope. The powder X-ray diffraction (XRD) study of silver nanocrystals after extensive purification was carried out with a Philips Model X'pert diffractometer using a Cu K_α radiation source (λ = 0.15418 nm). EELS measurements were obtained on an FEI Titan 80–300 TEM equipped with monochromator, an aberration corrector of the image-forming lens, and a high-resolution electron energy-loss spectrometer. The TEM was operated at 80 keV in both parallel illumination and scanning probe mode. Samples for the TEM were prepared by placing a drop of the nanorice solution onto a 3.05-mm-diameter thin-carbon-film TEM grid (Ted Pella).

RESULTS AND DISCUSSION

Typical Synthesis of Silver Nanorice Structures. Silver nanorice structures were synthesized by heating aged PEG stock solution containing $AgNO_3$ and PVP under ambient conditions. Stock solution was heated to, and kept at 70 °C in an oil bath for ∼2 h (stage I). When the yellow color disappeared, the nearly colorless solution was further heated at 100 °C for growth (stage II), which went through a series of color changes. No additional step for introducing shape-selected seeds or intentional addition of Cl^- or Br^- anions was involved. A fascinating feature is that light and dark stripes arranged in a complex manner along the long axis appear as a result of the presence of nanoscale FCC (111) twinning structure and multimode structural modulations arising essentially from the complicated stacking sequence. This is consistent with what we observed previously.[12]

To shed light on the growth kinetics of the silver nanorice under our typical synthesis conditions, the growth process was monitored by observing time-dependent color change of the solution and using the corresponding UV-Vis-NIR spectra and TEM images. The aged stock solution was yellow before heating (see Figure 1a, left), indicating the formation of silver NPs through the polyol reduction at room temperature, as supported by the TEM image (Figure 1c). After the solution was heated up to 70 °C, the yellow color gradually faded, mirroring the dissolution of the silver NPs, with the reaction proceeding. The solution progressed to be nearly colorless at t = 2 h, suggesting the lack of detectable silver NPs in the solution at this point.[16,19] Consistently, nearly no particles could be precipitated from the solution and purified even by high-speed centrifugation, because of their small sizes and/or low concentration. Because of that, the attempt to acquire clear TEM images of these NPs was not successful, because of the interference from excess PVP and PEG. The color reappeared after the temperature was increased to 100 °C and intensified with time. The color changed to green at 4.5 h, and finally to dark green (Figure 1a). The corresponding UV-Vis-NIR spectra

dx.doi.org/10.1021/cm3006875 | Chem. Mater. 2012, 24, 2339–2346

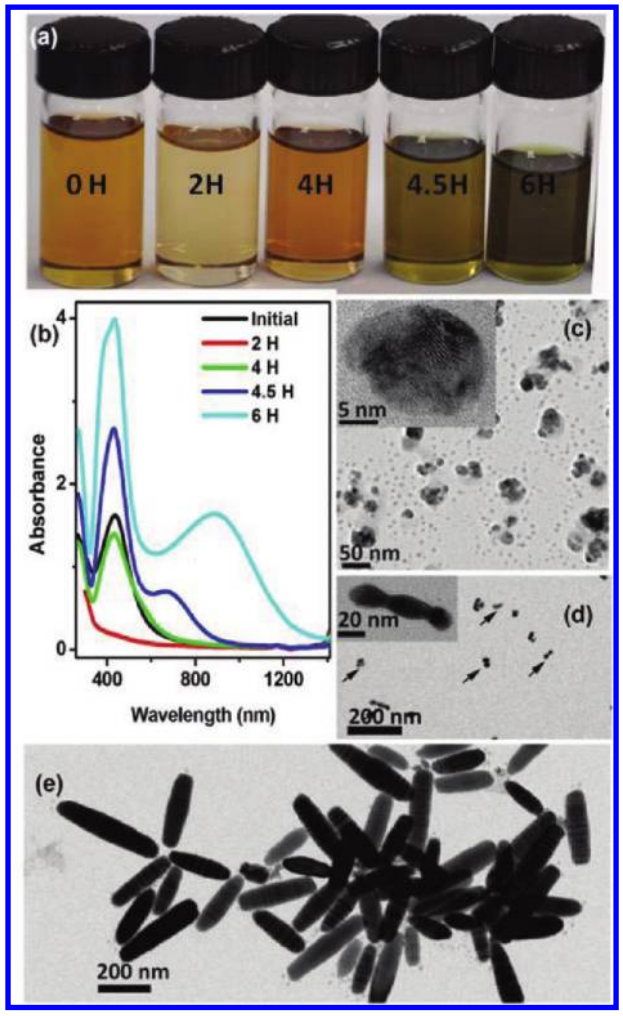

Figure 1. (a) Photographs of the reaction solution at 0, 2, 4, 4.5, and 6 h (from left to right), respectively, following typical synthesis procedures and (b) corresponding UV-Vis-NIR spectra. (c–e) TEM images of the products at different reaction times ((c) 0 h, (d) 4.5 h, and (e) 6 h). Insets of (c) and (d) are high-resolution TEM images.

are shown in Figure 1b. The SPR peak was centered at 438 nm at t = 0 h, disappeared at t = 2 h, and reappeared at t = 4 h. This peak originates from the SPR of the silver NPs.[16,19] Its evolution closely reflects the dissolution and reformation of considerable numbers of silver NPs. This observation is consistent with TEM observations (see Figure 1c and Figure S1 in the Supporting Information). It is worth mentioning that, in this "re-formed" sample, some large NPs and even NP agglomerates were also observed. At t = 4.5 h, a "new" peak situated at ~680 nm appears, indicative of the formation of one-dimensional silver nanostructures.[12] This has further been confirmed by TEM observations. Figure 1d shows the emergence of some incomplete nanorice-like particles, the contour of the individual NPs in which can be clearly identified. At t = 6 h, the sample obviously showed double peaks centered at 428 and 887 nm, corresponding to transverse and longitudinal resonances, respectively, because of the formation of the silver nanorice structures (see Figures 1b and 1e).[17]

Proposed Mechanism for Formation of Nanorice Structures. Based on the above observations, we propose a possible process herein for the shape evolution from the nearly spherically shaped nanocrystals to the nanorice structures. The scheme is illustrated in Figure 2.

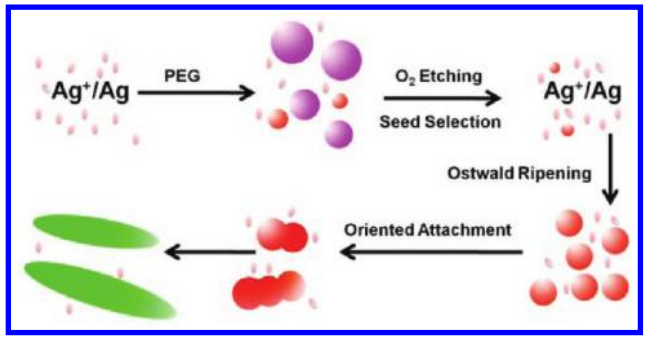

Figure 2. Proposed growth process of silver nanorice structures (red: single crystal; purple: twinned crystal; pink: Ag^0 or Ag^+; green: nanorice).

Silver ions in solution are reduced to form solid NPs by PEG at room temperature during the aging process. TEM studies indicate that such formed NPs exhibit a broad size distribution (1–45 nm; see Figure S2) and have single crystalline or twinned structures, consistent with that reported previously by Xia *et al.*[16] This indeed common observation of the copresence of single crystalline, singly twinned and multiply twinned morphologies in the same batch of silver NPs simply originates from the similarly relatively low energy barriers for forming these different morphologies, the distribution of which can be easily affected even by small thermal fluctuations.[16] Their chemical reactivity, however, is different and this difference is clearly mirrored from their different dissolution behavior at an elevated temperature of 70 °C in the presence of oxygen (in air). The higher reactivity of the twinned NPs, relative to that of the single crystalline NPs, leads to their preferential dissolution back into solution possibly because of oxidative etching, while the small single crystals remain intact. This process simultaneously causes the large decrease in the absorbance and, therefore, the disappearance of the solution color. The residual "robust" nanocrystals then serve as the seeds, slowly growing into primary NPs at ~4 h that subsequently attach with each other in an oriented fashion, i.e., by the so-called oriented attachment,[20–22] to form intermediate one-dimensional nanostructures, which eventually evolve into the typical nanorice structures. Thus, in the formation of the silver nanorice structures, the stage I is closely related to the seed selection process, while the stage II mainly the directional growth of the nanorice structures. The nanorice structures are the result of kinetically controlled growth at the intermediate temperature of 100 °C.

Oxygen-Enabled Seed Selection. The preferential dissolution of twinned structures has often been associated with oxidative etching. We assume, in our specific case, that oxygen in air may play a critical role in the etching in stage I (0–2 h). In order to test this hypothesis, the aged stock solution was bubbled by N_2 for 30 min and further pumped for 20 min to expel O_2 before the reaction (stages I and II) was allowed to proceed under the protection of N_2, using otherwise identical reaction conditions to those employed typically. In this case, the color-fading phenomenon was not observed. Instead, the color intensity kept increasing, in agreement with the steadily increased absorbance at ~440 nm (see Figures 3a and 3b). The sample only showed this single peak, and no additional peaks associated with one-dimensional nanostructures appeared, even after 5 h (stage I, 2 h; stage II, 3 h). These observations strongly suggest that the room-temperature-

dx.doi.org/10.1021/cm3006875 | *Chem. Mater.* 2012, 24, 2339–2346

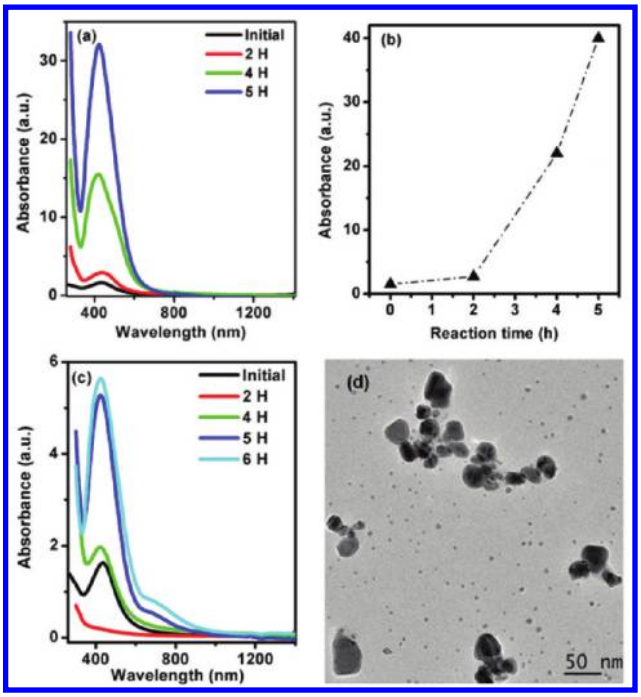

Figure 3. (a) UV-Vis-NIR spectra of the samples taken from the oxygen-free reaction at 0 (initial), 2, 4, and 5 h, respectively. (b) The intensity of the SPR peaks, as function of reaction time. (c) UV-Vis-NIR spectra of the samples taken from the reaction at 0 (initial), 2, 4, 5, and 6 h, respectively (the reaction was set in air for the first 2 h and then under N_2); and (d) TEM image of nanocrystals obtained at 6 h (the reaction was set in air for the first 2 h and then 4 h under N_2).

formed silver NPs were not dissolved at 70 °C (stage I) and only spherical (or quasi-spherical) silver NPs, instead of the nanorice structures, were formed as evidenced by TEM (see Figure S3 in the Supporting Information). It is clear that O_2 plays a crucial role in initiating the etching process, which is responsible for the seed selection that is a critical step toward the formation of the silver nanorice structures; when O_2 is expelled from the system, the silver nanorice simply could not be produced.

Although it is clear that oxygen-enabled seed selection takes place at 70 °C between 0 and 2 h, it is uncertain whether this seed selection continues at 100 °C and whether there are already sufficient numbers of seeds, from the 70 °C seed-selection process, to feed the growth of the silver nanorice. In order to address these points, the reaction was first allowed to proceed at 70 °C for 2 h in air and then O_2 was removed by bubbling N_2 through the solution before it was heated to 100 °C. The growth of silver NPs was again monitored using the UV-Vis-NIR spectrometry. It can be seen that, in this case, the evolution of the UV-Vis-NIR spectra, as shown in Figure 3c, was quite different from that shown in Figure 1b. Except for the characteristic SPR peak located at ~440 nm, only a small shoulder appeared at a longer wavelength of ~700 nm after the reaction lasted as long as 6 h. This shoulder can be ascribed to the strong coupling of the NPs, because of their random aggregation, instead of the formation of the nanorice, as supported by TEM (Figure 3d). It seems that the oxygen-enabled seed selection continues in stage II and is an important shape-directing variable for the formation of the nanorice; the inhibition of this process in either stage I or II by removing oxygen significantly impedes the nanorice growth. Quite likely, the seeds formed in stage I are not enough for the nanorice growth in stage II. These results confirm that the presence of O_2 in both stages I and II is absolutely required for the synthesis of nanorice.

The concomitant seed selection during the growth period readily distinguishes the current nanorice synthesis from a commonly used two-step approach, the so-called "seeded growth" method. In that method, the nucleation process is intentionally separated from the growth stage, whereby the growth takes place on existing seeds and no new seeds will be formed in later stages.

Oriented-Attachment Dominated Growth. Once the seeds are formed, in most cases, they grow through the gradual deposition of monomers (atoms or ions) on the surface, and finally develop into different shapes.[16] Ostwald ripening is normally involved in this process,[22−25] with diffusion being the growth-controlling factor. A much less-occurring growth mechanism is the oriented attachment, which is related to the direct self-organization of particles by joining at particular faces and sharing a common crystallographic orientation.[26,27] Although it remains challenging to describe the kinetics of the oriented attachment process involving many particles satisfactorily, some models (including a polymerization model) have been proposed, which fit the oriented attachment growth well via the oriented attachment of a few particles.[28] In our system, the formation of the silver nanorice seems to be dominated by this spontaneous, oriented attachment, as clearly evidenced by the contour of constituent NPs in many intermediate particles during their shape development toward the final nanorice structures (Figure 1d). At higher magnifications, the constituent, primary NPs can be straightforwardly defined. Figure 4 shows two transient silver particles,

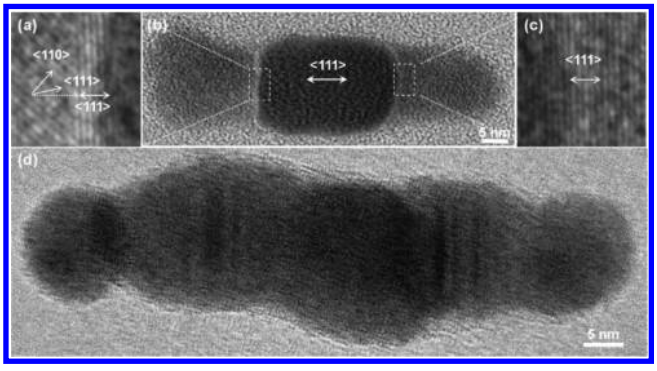

Figure 4. Oriented attachment of silver NPs. Panels (a) and (c) are high-resolution TEM images of the selected area highlighted by the rectangles in (b).

which are composed of three or five small, primary NPs, before they eventually evolve into the smooth nanorice structures. While it seems that the silver NPs are attached more or less along the ⟨111⟩ direction, the joining surfaces do not necessarily always share exactly the same orientation; there may be a misorientation angle between them. These particles may then realign themselves with respect to each other to make better alignment along the ⟨111⟩ direction during the further growth (Figure 5) to form single crystals.[28] As an interesting demonstration of the coexistence of imperfect and perfect junctions in a single rice structure, Figure 4a shows a certain degree of misorientation of two grains, while Figure 4c clearly shows that two grains are highly coherent in their lattice fringes across the interface. Despite the dominance of the oriented

dx.doi.org/10.1021/cm3006875 | *Chem. Mater.* 2012, 24, 2339−2346

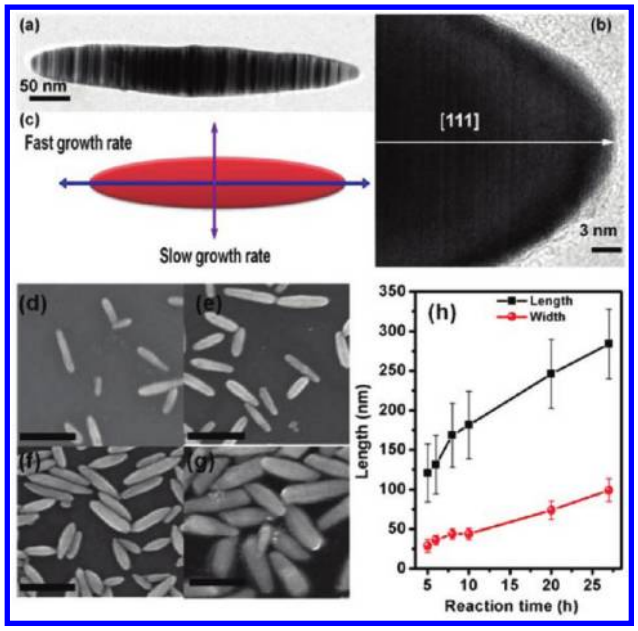

Figure 5. (a) TEM image of a silver nanorice. (b) High-resolution TEM image of the end of (a). (c) Illustration of growth rates during the formation of nanorice structures. SEM images of the samples synthesized at 100 °C (stage II) for the total reaction time of (d) 5 h, (e) 6 h, (f) 8 h, and (g) 20 h. All scale bars are 200 nm. (h) The variation of the length and diameter of the silver nanorice structures with total reaction times of 5, 6, 8, 10, 20 h, and 27 h, respectively, during the growth process at 100 °C.

attachment, the Ostwald ripening cannot be completely excluded. Considering that most of these primary NPs are larger than 10 nm in diameter (see Figures S4 and S5 in the Supporting Information,) together with the extremely small size of the seeds, as supported by the featureless UV-Vis-NIR spectrum at 2 h, it can be speculated that Ostwald ripening, accompanied by continued seed selection, is at least responsible for the initial seed growth into the primary NPs, although its role in the key developing period (≥4.5 h) of the nanorice structures dwindles or is hidden. The reason that the growth mode of the oriented attachment is preferred in our case is perhaps due to the lower energy barrier involved for adjoining already-formed NPs than adding monomers via the diffusion in solution at this specific temperature of 100 °C.

Then an interesting question arises: why the primary NPs prefer to attach with each other in an oriented way, instead of randomly, as observed in most cases? The answer perhaps consists in the way the ligands are capping the NPs. It has been reported that PVP can selectively bind to the {100} facets of silver nanocrystals and slow down their growth rate,[10] while the {111} faces are less passivated by PVP and thus much more reactive during the reaction. As a highly likely consequence of this selective adsorption of the capping molecules, the anisotropic growth of nanocrystals on certain crystal planes is anticipated. In our specific case, it proceeds through adjoining the poorly passivated {111} facets of adjacent primary NPs, resulting in an elongation of the ⟨111⟩ direction, as demonstrated by high-resolution TEM studies (see Figures 5b and 5c). Clearly, the growth is controlled by kinetics governing the NP attachment along the ⟨111⟩ direction, versus that along other crystallographic directions as well as diffusion-controlled monomer deposition. In addition, the nanorice structures were found to have the typical (111) twinning structure,[12] with the commonly appearing sample size being as small as a few nanometers (Figure 5a and b). The formation of complex defect structures including closely spaced twins and stacking faults has been noticed in the oriented-attachment dominated crystal growth and has been interpreted as a natural outcome of decreasing the internal energy of the crystals for stabilizing their structure.[29]

Even though the lateral growth is not preferred versus the remarkable one-dimensional growth along the ⟨111⟩ direction, because of the better PVP passivation, it is not entirely obstructed. The increase of the lateral dimension becomes more apparent in examining the nanorice structures at extended periods of reaction time (≥20 h) and comparing them to those typically synthesized after several hours, as shown by the SEM images in Figures 5d−5g. For better comparison, the average length and diameter in the central part of the nanorice structures at different reaction time are summarized in Figure 5h. Despite the broad length distribution, the trend can be identified. It can be seen that both longitudinal and lateral dimensions increased with time. The growth rate along the long axis was considerably higher than that in the later period, because of the running out of the primary NPs at longer reaction time. Even though the growth rate along the long axis became slower in the later stage, it was still higher than that along the short axis. In fact, the growth rate along the ⟨111⟩ direction was consistently higher than that along the short axis throughout the investigated time interval. We believe that the Ostwald ripening is dominant in the slow, lateral growth of the nanorices. Therefore, although the key, one-dimensional growth is governed by the oriented attachment, the overall growth of the nanorice, including both lateral and longitudinal, involves the combination of both growth pathways. Similar growth pathways have been reported for anisotropic titanium dioxide structures.[30]

Temperature Effect. Temperature effect was also examined in order to provide more insights into the kinetically controlled, anisotropic growth process. In general, higher temperature not only accelerates nanocrystal growth, but also alters the difference of the growth rates on crystallographically different planes, and thereby the final geometry of nanocrystals. It may also change the growth mechanism as well. Two higher reaction temperatures, 120 and 160 °C, were employed in stage II, following the typical seed-selection process at 70 °C for 2 h. The growth of silver nanocrystals appeared to be strongly affected by the reaction temperature. As presented in Figure S6a in the Supporting Information, the evolution of the SPR peak position of the samples generated at 120 °C was similar to that of the 100 °C samples. However, as expected, the growth rate of the nanocrystals at 120 °C was much faster. The product clearly showed typical double peaks of one-dimensional silver nanostructures as early as 1 h at 120 °C (total reaction time, including stage I, is 3 h), other than 2.5 h at 100 °C (total reaction time, including stage I, is 4.5 h). Correspondingly, Figures 6a and 6c clearly show the formation of nanobars with reaction time as short as 1 h at 120 °C. They were similar to the nanorice structures synthesized at 100 °C in the shape and growth direction, whereas without obvious tips at two ends. Xia *et al.* have demonstrated that the seed selection process highly depends on the reaction temperature.[15,31] Elevated temperature will accelerate the etching of the twinned crystals and thereby the seed selection process. As a result, 120 °C is more efficient than 100 °C in generating large amounts of single crystal seeds to feed the crystal growth in the way of the oriented

dx.doi.org/10.1021/cm3006875 | *Chem. Mater.* 2012, 24, 2339−2346

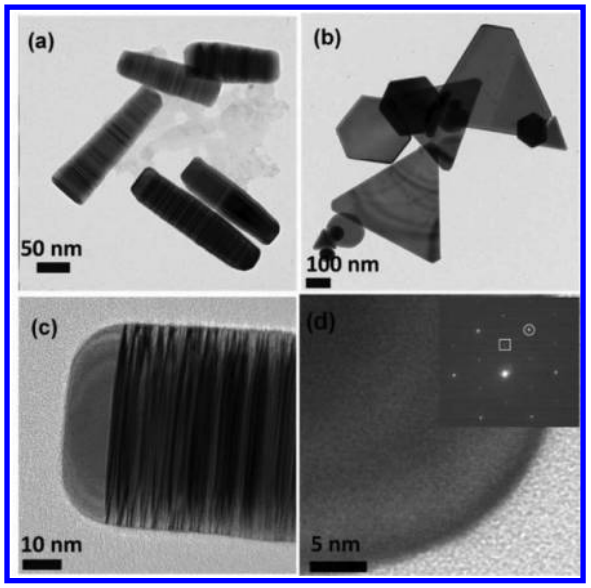

Figure 6. TEM images of the samples synthesized at (a and c) 120 °C with a total reaction time of 3 h 25 min, and at (b and d) 160 °C with total reaction time of 4 h. Inset of panel (d) is the SAED pattern of a silver nanoplate. The intense spot marked by a circle is due to the {220} reflection and the weak spot marked by a square is indexed as $^{1}/_{3}${422}.

attachment. On the other hand, the growth from the single crystal seeds to the primary NPs via the Ostwald ripening is also expected to be faster at the elevated temperature of 120 °C. More rapid seed generation, together with faster growth, leads to the earlier emergence of the one-dimensional structure (i.e., the nanobars). The absence of the tips in this sample perhaps is related to the increased quality (and, thus, stability) of single-crystal NPs synthesized at a higher temperature.[32] It was further noted that the single crystals capping the nanobars were typical of the nearly flawless FCC structure, quite different from what we found for the nanorice structures.[12] It seems that there is a strong correlation between the HCP phase and the tip morphology in the nanorice structures as the HCP phase is often present in their tips. It is possibly due to that the HCP phase has a more stable surface configuration at a certain shape and size range, and the increasing ratio of surface atoms at the tip favors the presence of the HCP phase. Although absent at the two ends, the HCP phase was still present in the nanobars (see Figure S7 in the Supporting Information). In addition to characteristic FCC diffraction peaks, a small peak ascribed to the HCP phase diffraction is present in both 100 and 120 °C samples, indicating that FCC and HCP phases coexist in these two samples. Despite the slight structural modification at the ends, the dominant growth still occurs along the ⟨111⟩ direction. It is clear that although the growth rate along all directions is expected to increase with increasing temperature, the growth rate in other directions still cannot compete with that along the ⟨111⟩ direction, the same as that occurs at 100 °C.

In clear contrast, when the reaction temperature in stage II was further increased to 160 °C, only one SPR peak was identified at a wavelength of ~400 nm at the total reaction time of 4 h. It was, however, accompanied by a dramatically increased absorption at longer wavelengths up to 1400 nm, which is the maximum wavelength measured herein (see Figure S6b in the Supporting Information). Figures 6b and 6d show that the reaction at 160 °C led to a sample with a completely different morphology from that at 100 and 120 °C. No one-dimensional nanostructures were formed. The sample showed a very broad size distribution and large shape anisotropies; it was essentially a mixture of highly faceted triangular and hexagonal two-dimensional plates and spherical (or quasi-spherical) NPs (see Figure S8 in the Supporting Information), all having the pure FCC crystal structure (see Figure S7 in the Supporting Information). Moreover, the triangular plates were more or less truncated at corners. Selected area electron diffraction (SAED) (Figure 6d, inset) reveals that both triangular and hexagonal plates were mainly bounded by {111} crystal planes, in agreement with what has been reported so far for silver and gold plates.[33] In addition to brighter spots from the {220} reflection, the weak spots from the $^{1}/_{3}${422} reflection were also observed, suggesting the presence of parallel twin planes in the individual plate.[33] The growth of these plates should be due to the diffusion-controlled, favorable deposition of adatoms at the re-entrant grooves created by the twin plane.[33] The loss of the difference in the selective binding of PVP to different crystal planes at elevated temperature may also contribute to this growth process. It is clear that although the growth of all the anisotropic nanostructures is kinetically controlled, the dominant formation mechanism at 100 and 120 °C is completely different from that at 160 °C, with the former being the oriented attachment, and the latter being the diffusion-controlled deposition. The growth in the ⟨111⟩ direction also changes from the most favorable to a largely hindered one. Obviously, temperature plays an important role in varying the growth mechanism and growth direction.

SPR Sensing of Nanorice Structures. The SPR sensitivity of the nanorice structures to the refractive index of their surrounding medium was studied by examining the shift of the SPR peak of the nanorice structures immersed in different dielectric media. As shown in Figure 7a, both the transverse and

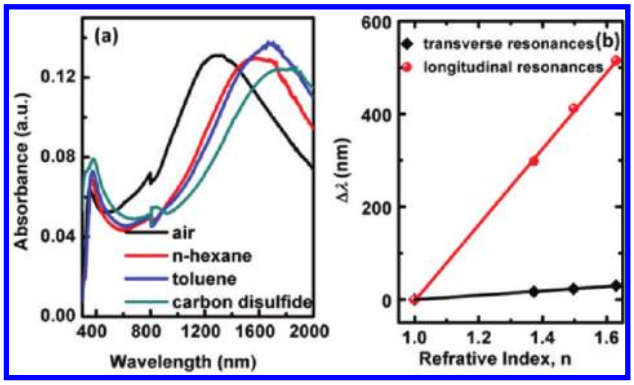

Figure 7. SPR sensing using silver nanorice structures: (a) UV-Vis-NIR spectra of a monolayer–nanorice film immersed in different dielectric media and (b) the peak shift of the transverse and longitudinal SPR bands as a function of the local refractive index. The SPR sensitivity based on the longitudinal and transverse plasmons is 820.6 and 47.3 nm/RIU, respectively.

longitudinal plasmons of the nanorice structures exhibited red shifts with increasing refractive index from 1 (air) to 1.63 (carbon disulfide), as expected from the Mie scattering theory.[34,35] Figure 7b plots the peak shift of the transverse and longitudinal SPR bands ($\Delta\lambda_{trans}$ and $\Delta\lambda_{longi}$) as a function of the refractive index. Both peak shifts showed the same linear dependence on the refractive index, yet with quiet different

dx.doi.org/10.1021/cm3006875 | Chem. Mater. 2012, 24, 2339–2346

slopes, or sensitivity factors, being 820.6 nm RIU^{-1} (RIU = refractive index unit) and 47.3 nm RIU^{-1} for the longitudinal and transverse SPR bands, respectively. It is clear that the longitudinal plasmon is remarkably more sensitive, by 17 times, to the environmental change than the transverse plasmon. This longitudinal SPR sensitivity of 820.6 nm RIU^{-1} is much higher than that of gold and silver nanorods reported previously.[34,35] As a matter of fact, it is comparable to the highest value (achieved on a Fe_2O_3/Au hybrid structure) reported so far for one-dimensional plasmonic nanostructures,[36] to the best of our knowledge. The SPR sensitivity of nanostructures to refractive index is affected by multiple factors, such as the material, size, and shape of nanostructures.[35] For example, compared to gold and other noble-metal nanostructures, the SPR shift of silver nanostructures with refractive index is found to be always much larger.[35] In addition, in general, nanostructures with sharper geometries, larger aspect ratios, and SPR peaks at longer wavelength (e.g., in the NIR region) show higher sensitivity to the variation of the refractive index of their immediate surroundings.[34,35] The very high sensitivity of the nanorice structures developed herein is thus attributed to not only their material, but also their sharp apexes, large aspect ratios, and long wavelength (in the NIR) of their SPR peaks. Such high environmental sensitivity of the longitudinal plasmon of the nanorice structures makes them an ideal platform for monitoring local environmental changes during chemical and biological processes.

Multipolar Resonance Imaging. Multiple plasmonic resonances in a single nanorice structure were imaged by acquiring EELS signals from a scanning electron probe in the TEM system. The plasmon oscillations were excited in the TEM system impulsively by the transient field of the fast electron.[37−40] By performing EELS, we can measure small changes in the kinetic energy of the incident electron beam after having passed through or near a thin specimen, providing material-sensitive information in the form of the amount of energy that has been transferred to the specimen.[41] Figure 8 shows the rectangular region enclosing a nanorice structure, 304 nm long and 64 nm diameter at the center, from which EELS signals were acquired. The EELS signal is very sensitive to the position of the probe with respect to the structure, featuring peaks at (1.00, 1.75, 2.32, 3.47) eV energy loss at different locations near the surface of the nanorice (Figure 8b,c). These peaks arise from the loss of energy of the electron probe to the excitation of plasmonic resonances, which can be mapped by selectively filtering the scattering intensity belonging to a narrow energy loss centered on each peak (Figure 8d). From the energy-filtered maps, we observed a standing wave pattern in the intensity across the long axis of the nanorice, belonging to the interference of counter-propagating, longitudinal plasmon waves with successive mode orders (m = 1−3) resolved at increasing energy loss. We also resolved the transverse surface plasmon resonance at 3.47 eV, which is strongly confined to the surface of the nanorice. These observations indicate that the nanorice structures exhibit behavior qualitatively similar to that of purely cylindrical silver nanorods,[42] although the specific energies of the particular resonances are shifted with respect to a silver cylinder of the same length (304 nm long and 41 nm diameter), whose resonance energies were measured at (0.70, 1.46, 2.05) eV. The resonances can be tuned by changing the length of the nanorice via varying reaction time.

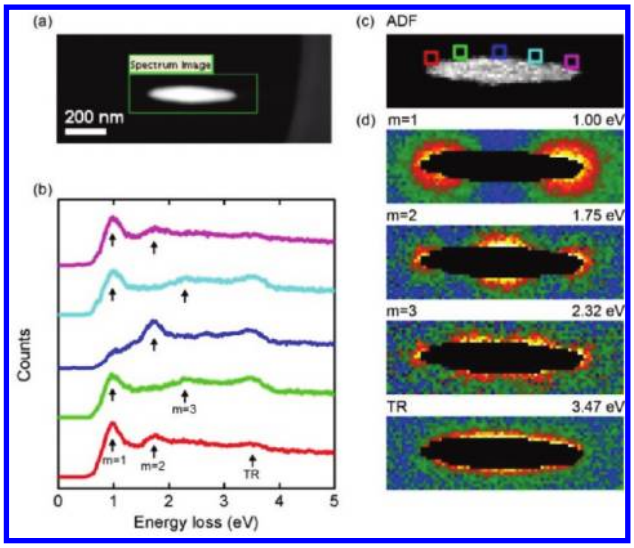

Figure 8. Nanoscale EELS spectroscopy of a nanorice structure. (a) A rectangular region surrounding a nanorice structure, supported on a thin carbon film, defines the limits of the region over which the electron probe is scanned. (b) The EELS signal (after zero loss peak subtraction) varies with the position of the probe shown in panel (c). (d) Multiple plasmonic resonances excited in the nanorice are mapped by selectively filtering the scattering intensity belonging to each peak in the EELS signal. The first three resonances (m = 1−3) are resolved at 1.00, 1.75, and 2.32 eV, and the transverse surface plasmon resonance, tightly bound to the surface of the nanorice, is resolved at 3.47 eV.

■ CONCLUSIONS

Interesting silver nanorice structures have been synthesized on a large scale by a polyol process and their formation process is investigated. It is found that the seed selection process, based on the oxidative etching of the twinned crystals, is an indispensable step for the growth of the nanorice structures and oxygen plays a critical role in this seed selection process. The major shape development stage of the nanorice structures is dominated by the oriented attachment along the ⟨111⟩ direction, directed by the nonuniform capping of PVP on different facets. The Ostwald ripening is responsible for the seed growth into the primary NPs and the lateral growth of the nanorice structures, albeit it is not straightforwardly apparent in the early stage of the anisotropic growth of the nanorice. Slightly increasing temperature shows the acceleration effect on the one-dimensional growth along the ⟨111⟩ direction, while further increase in temperature leads to the disappearance of the one-dimensional shape and induces the formation of highly faceted, two-dimensional, truncated triangular and hexagonal plates mainly bound by low-energy faces of {111}. The growth mechanism of these two-dimensional plates is remarkably different from that of the nanorice structures. Instead of the oriented attachment, their growth is controlled by diffusion and dictated by the twin plane. The longitudinal SPR of the nanorice synthesized herein is highly sensitive to the surrounding dielectric medium, which makes them highly promising for sensor applications. Furthermore, in addition to the longitudinal resonance, the multipolar resonances in individual nanorcies are mapped in real space, using the high-resolution EELS technique.

dx.doi.org/10.1021/cm3006875 | *Chem. Mater.* 2012, 24, 2339−2346

■ ASSOCIATED CONTENT

Supporting Information

Additional figures. This material is available free of charge via the Internet at http://pubs.acs.org.

■ AUTHOR INFORMATION

Corresponding Author

*E-mails: hongxingxu@aphy.iphy.ac.cn (H.X.), ma@emt.inrs.ca (D.M.).

Notes

The authors declare no competing financial interest.

■ ACKNOWLEDGMENTS

We acknowledge Liangming Tong for the valuable comments and discussions. This work was supported by the funds from the Natural Sciences and Engineering Research Council of Canada and Fonds de la Recherche Sur La Nature Et Les Technologies. Financial support from the Merit Scholarship Program for Foreign Students from the Ministère de l'Éducation, du Loisir et du Sport du Québec is greatly appreciated. This work was also supported by the NSFC Grants (Nos.10625418, 10874233 and 11004237), MOST Grants (Nos. 2006DFB02020 and 2009CB930700), "Knowledge Innovation Project" (KJCX2-EW-W04) of CAS.

■ REFERENCES

(1) Wen, F.; Zhang, W.; Wei, G.; Wang, Y.; Zhang, J.; Zhang, M.; Shi, L. *Chem. Mater.* **2008**, *20*, 2144.
(2) Jin, R.; Cao, Y.; Mirkin, C. A.; Kelly, K. L.; Schatz, G. C.; Zheng, J. G. *Science* **2001**, *294*, 1901.
(3) Novak, J. P.; Brousseau, L. C.; Vance, F. W.; Johnson, R. C.; Lemon, B. I.; Hupp, J. T.; Feldheim, D. L. *J. Am. Chem. Soc.* **2000**, *122*, 12029.
(4) Chattopadhyay, S.; Lo, H. C.; Hsu, C. H; Chen, L. C.; Chen, K. H. *Chem. Mater.* **2005**, *17*, 553.
(5) Liang, H. Y.; Li, Z. P.; Wang, W. Z.; Wu, Y. S.; Xu, H. X. *Adv. Mater.* **2009**, *21*, 4614.
(6) Wang, W.; Li, Z.; Gu, B.; Zhang, Z.; Xu, H. *ACS Nano* **2009**, *3*, 3493.
(7) Lee, S.; Mayer, K. M.; Hafner, J. H. *Anal. Chem.* **2009**, *81*, 4450.
(8) Maillard, M.; Giorgio, S.; Pileni, M. P. *Adv. Mater.* **2002**, *14*, 1084.
(9) Sun, Y.; Yin, Y.; Mayers, B. T.; Herricks, T.; Xia, Y. *Chem. Mater.* **2002**, *14*, 4736.
(10) Wiley, B.; Chen, Y.; Mclellan, J. M.; Xiong, Y.; Li, Z. Y.; Ginger, D.; Xia, Y. N. *Nano Lett.* **2007**, *7*, 1032.
(11) Chen, S.; Carroll, D. L. *Nano Lett.* **2002**, *2*, 1003.
(12) Liang, H. Y.; Yang, H. X.; Wang, W. Z.; Li, J. Q.; Xu, H. X. *J. Am. Chem. Soc.* **2009**, *131*, 6068.
(13) Liang, H. Y.; Wang, W. Z.; Huang, Y. Z.; Zhang, S. P.; Wei, H.; Xu, H. X. *J. Phys. Chem. C* **2010**, *114*, 7427.
(14) Komarneni, S.; Li, D. S.; Newalkar, B.; Katsuki, H.; Bhalla, A. S. *Langmuir* **2002**, *18*, 5959.
(15) Wiley, B.; Sun, Y.; Mayers, B.; Xia, Y. N. *Chem.—Eur. J.* **2005**, *11*, 454.
(16) Wiley, B.; Herricks, T.; Sun, Y. G.; Xia, Y. N. *Nano Lett.* **2004**, *4*, 1733.
(17) Im, S. H.; Lee, Y. T.; Wiley, B.; Xia, Y. N. *Angew. Chem., Int. Ed.* **2005**, *44*, 2154.
(18) Wei, H.; Reyes-Coronado, A.; Nordlander, P.; Aizpurua, J.; Xu, H. X. *ACS Nano* **2010**, *4*, 2649.
(19) Peng, S.; McMahona, J. M.; Schatzb, G. C.; Graya, S. K.; Sun, Y. *Proc. Natl. Acad. Sci. U.S.A.* **2010**, *107*, 14530.
(20) Penn, R. L.; Banfield, J. F. *Science* **1998**, *281*, 969.
(21) Penn, R. L.; Banfield, J. F. *Am. Mineral.* **1998**, *83*, 1077.
(22) Wagner, C. *Z. Elektrochem.* **1961**, *65*, 581.
(23) Lifshitz, I. M.; Slyozov, V. V. *J. Phys. Chem. Solids* **1961**, *19*, 35.
(24) Talapin, D. V.; Rogach, A. L.; Haase, M.; Weller, H. *J. Phys. Chem. B* **2001**, *105*, 12278.
(25) Zhao, H. G.; Chaker, M.; Ma, D. *J. Phys. Chem. C* **2009**, *113*, 6497.
(26) Huang, F.; Zhang, H.; Banfield, J. F. *Nano Lett.* **2003**, *3*, 373.
(27) Zhang, J.; Lin, Z.; Lan, Y.; Ren, G.; Chen, D.; Huang, F.; Hong, M. *J. Am. Chem. Soc.* **2006**, *128*, 12981.
(28) Ribeiro, C.; Lee, E. J. H.; Longo, E.; Leite, E. R. *Chem. Phys. Chem.* **2006**, *7*, 664.
(29) Huang, F.; Zhang, H. Z.; Banfield, J. F. *J. Phys. Chem. B* **2003**, *107*, 10470.
(30) Zhan, H.; Yang, X.; Wang, C.; Liang, C.; Wu, M. *J. Phys. Chem. C* **2010**, *114*, 14461.
(31) Lu, X.; Rycenga, M.; Skrabalak, S. E.; Wiley, B.; Xia, Y. N. *Annu. Rev. Phys. Chem.* **2009**, *60*, 167.
(32) Wang, B.; Fei, G. T.; Zhou, Y.; Wu, B.; Zhu, X.; Zhang, L. *Gryst. Growth Des.* **2008**, *8*, 3073.
(33) Lofton, C.; Sigmund, W. *Adv. Funct. Mater.* **2005**, *15*, 1197.
(34) Chen, H.; Kou, X.; Yang, Z.; Ni, W.; Wang, J. *Langmuir* **2008**, *24*, 5233.
(35) Sekhon, J. S.; Verma, S. S. *Plasmonics* **2011**, *6*, 311.
(36) Wang, H.; Brandl, D. W.; Le, F.; Nordlander, P.; Halas, N. J. *Nano Lett.* **2006**, *6*, 827.
(37) N'Gom, M.; Ringnalda, J.; Mansfield, J. F.; Agarwal, A.; Kotov, N.; Zaluzec, N. J.; Norris, T. B. *Nano Lett.* **2008**, *8*, 3200.
(38) Nelayah, J.; Kociak, M.; Stephan, O.; Abajo, F. J. G.; Tence, M.; Henrard, L.; Taverna, D.; Pastoriza-Santos, I.; Liz-Marzan, L. M.; Colliex, C. *Nat. Phys.* **2007**, *3*, 348.
(39) Guiton, B.; Iberi, V.; Li, S.; Leonard, D. N.; Parish, C. M.; Kotula, P. G.; Varela, M.; Schatz, G. C.; Pennycook, S. J.; Camden, J. P. *Nano Lett.* **2011**, *11*, 3482.
(40) Koh, A. L.; Fernández-Domínguez, A. I.; McComb, D. W.; Maier, S. A.; Yang, J. K. W. *Nano Lett.* **2011**, *11*, 1323.
(41) Egerton, R. F. *Electron Energy-Loss Spectroscopy in the Electron Microscope*, Second ed.; Plenum Press: New York, 1996.
(42) Rossouw, D.; Couillard, M.; Vickery, J.; Kumacheva, E.; Botton, G. A. *Nano Lett.* **2011**, *11*, 1499.